PCCP

ROYAL SOCIETY OF CHEMISTRY

PAPER

View Article Online
View Journal | View Issue

Cite this: *Phys. Chem. Chem. Phys.*, 2026, **28**, 4954

Effect of specific interactions on the double layer capacitance of concentrated ionic systems

Oksana Patsahan [a] and Alina Ciach *[b]

Received 22nd November 2025,
Accepted 16th January 2026

DOI: 10.1039/d5cp04532k

rsc.li/pccp

The effect of non-coulombic short-range (SR) interactions on the double-layer capacitance in concentrated ionic systems is studied on a general level within mesoscopic density–functional theory. We improve the formula for the capacitance obtained in our previous work by adding a factor representing the charge of the electrode consistent with the formalism of the mesoscopic theory. Perfect agreement with the Debye capacitance for dilute electrolytes, and a fair agreement with simulations for concentrated electrolytes is obtained for the restricted primitive model (RPM). Explicit formulas for the potential of zero charge (PZC) and the capacitance at the PZC are obtained for the RPM with additional attractive SR interactions between like ions and with different SR cation–electrode and anion–electrode interactions. The capacitance at the PZC has the form of the original Helmholtz capacitance, with the distance of the virtual monolayer of counterions from the electrode that has the same dependence on the lengths characterizing the oscillatory decay of the charge density as in the RPM. These lengths, however, depend significantly on the SR interactions.

I. Introduction

The structure of a double layer in concentrated ionic systems is significantly different from that in dilute electrolytes. In dilute electrolytes, the charge–density decays with the distance z from the electrode as $c(z) \propto \exp(-z/\lambda_D)$, where the Debye screening length, λ_D, is inversely proportional to $\sqrt{\rho}$, with ρ denoting the density of ions.[1,2] The charge of the electrode is neutralized by the charge of the double layer, and the Debye capacitance concerning a small voltage at the electrode is $C_D = \epsilon/(4\pi\lambda_D)$, where ϵ is the dielectric constant.

In concentrated ionic systems, however, the double layer consists of alternating oppositely charged layers, and the charge density decays as $c(z) \propto \exp(-\alpha_0 z)\sin(\alpha_1 z + \theta)$.[3–7] The decay length α_0^{-1} increases with increasing ρ, *i.e.* it depends on ρ in a completely different way than λ_D does.[7–9] Hence, the Debye length λ_D is no longer associated with the double-layer thickness. The charge of the electrode is compensated by the integral of $c(z)$ that depends on the two inverse length scales α_0 and α_1. Because λ_D does not describe the complex distribution of ions in this case, the capacitance must differ from C_D.

Rather surprisingly, it was observed in ref. 10 and 11 that the very first formula for the double-layer capacitance proposed by Helmholtz, $C = \epsilon/(4\pi L)$, where L is the distance from the electrode of a fixed layer of counterions, quite well describes the capacitance of concentrated electrolytes. In ref. 11 it was shown that alternating layers of counterions and coions can be replaced by a virtual monolayer of counterions placed at the distance L from the electrode that depends on α_0, α_1. In ref. 11 the formula

$$C = \frac{\epsilon(\alpha_0^2 + \alpha_1^2)}{4\pi a} \quad (1)$$

was obtained for the restricted primitive model (RPM) of oppositely charged hard spheres with diameter a in structureless solvent. In (1), α_0 and α_1 are dimensionless (in $1/a$ units). However, comparison with simulations for the RPM[12] showed that C given by (1) was overestimated by a factor $\sim$3. The discrepancy between the theoretical and simulation results was attributed to the microscopic structure at the electrode that on the mesoscopic level is not described with sufficient precision, and it was postulated that the right hand side in eqn (1) should be multiplied by a factor $f \sim 1/3$.

In this work, we propose a very simple definition for the factor f within our mesoscopic theory, and obtain fair quantitative agreement with simulations. Next, we use this definition in determining the effect of short-range (SR) interactions on the capacitance at the potential of zero charge (PZC), which is our main goal in this work.

The effect of the SR interactions was studied in particular in ref. 13–22, but in the majority of theoretical studies on the capacitance, the specific SR interactions are neglected. The theoretical results obtained for the potential Ψ are compared

[a] *Yukhnovskii Institute for Condensed Matter Physics of the National Academy of Sciences of Ukraine, 1 Svientsitskii St., 79011 Lviv, Ukraine*
[b] *Institute of Physical Chemistry, Polish Academy of Sciences, 01-224 Warszawa, Poland. E-mail: aciach@ichf.edu.pl*

with the experimental results obtained for $\Psi - \Psi_{PZC}$. Ψ_{PZC} is the potential at the uncharged electrode in contact with the ionic solution. It is induced by a selectivity of the electrode that attracts more strongly one type of ion by the SR forces. PZC is a signature that the SR anion–electrode and cation–electrode interactions are different. The van der Waals interactions between the ions in IL and metallic electrodes can be strong, as measured for the gold electrode and fluorine-free phosphonium-based ionic liquids in ref. 23. A signature of the SR ion–ion interactions in the bulk is the phase transition between ion-rich and ion-poor phases, *i.e.* the miscibility gap, with the critical density of ions similar to the critical density of the gas–liquid phase separation in neutral fluids.[24,25] The strength of these interactions is proportional to the critical temperature of this transition. The SR interactions include direct van der Waals interactions between the ions, H-bond formation, as well as effective solvent-mediated interactions in the approach with implicit solvent.

The strength and range of the SR interactions strongly depend on the type of the system. In the case of organic ions dissolved in water, the solvent-induced effective interactions are stronger than the van der Waals interactions. These forces having rather complex origins are called hydrophobic attraction[26] and are responsible for aggregation of hydrophobic particles (or ions) in water. In particular, in systems such as aqueous solutions of 1-butyl-3-pentylimidazolium bistriflimide, 1-butyl-3-isopentylimidazolium bistriflimide, and 1-butyl-3-cyclopentylimidazolium bistriflimide,[25] hydrophobic attraction leads to phase separation, with the critical temperature around 400 K.

In general, the SR interactions may significantly influence the distribution of the ions, as observed for the so-called antagonistic salts,[17–19] or for water in salt systems.[20–22] In particular, the inverse lengths α_0 and α_1 may depend on the SR interactions, thus leading to the dependence of C on the SR interactions as well. A notable example is the concentrated lithium bis(trifluoromethylsulfonyl)-imide (LiTFSI) in water, where the hydrophobic attraction between organic anions is strong enough to induce their aggregation and separation from hydrated Li^+, by which alternating oppositely charged regions of mesoscopic size are formed.[20–22]

In order to answer the question of how the SR interactions influence the capacitance on a general qualitative level, we consider in this work the RPM with additional SR interactions of a simple mathematical form but with various strengths. We do not try to model any particular system, but rather to obtain a general qualitative picture for mixtures of ions with neutral solvents that can phase separate into ion-poor and ion-rich phases. More complex systems, such as binary solvents, are not considered here. We calculate the charge profile and determine the capacitance at the PZC within our mesoscopic version of the density functional theory.[7]

In Section II A, we introduce the interaction potentials and estimate the physical range of the parameters in the SR interaction potential. In Section II B, we apply the formalism of the mesoscopic DFT to the RPM+SR model and describe the approximations that we use for determination of the structure in the bulk. The methods and approximations used in studies of the effect of the electrode in this model are described in Section II C. Results for the bulk are presented in Section III A. Capacitance in the pure RPM with the new definition of the charge at the electrode within our mesoscopic theory is obtained for dilute and concentrated electrolytes in Section III B. The results for the charge profile, PZC and capacitance in the RPM+SR model are shown in Section III C. The last section contains concluding remarks.

II. Model and theory

A. Model

In our simplified model, the solvent is characterized by the dielectric constant ϵ. In addition, it may induce effective interactions between the ions. We assume that in the effectively two-component system, the pair interaction potentials between two ions with hard spheres of diameter a, for $r > a$ can be presented in the form:

$$V_{ij}(r) = V_{ij}^{C}(r) + V_{ij}^{A}(r)\delta_{ij}^{Kr}, \quad i,j = +,- \tag{2}$$

Here, $V_{ij}^{C}(r)$ are the truncated Coulomb potentials between the ions with the signs i and j in the system where the overlap of the hard cores is forbidden. As a length unit we choose the ion diameter a. The truncated Coulomb potentials are

$$\beta V_{ij}^{C}(r^*) = ij\frac{l_B\theta(r^*-1)}{r^*}, \tag{3}$$

where $r^* \equiv r/a$,

$$l_B = \frac{1}{T^*} = \beta E_C, \quad E_C = \frac{e^2}{a\epsilon}, \tag{4}$$

and $\beta = 1/k_BT$ with k_B and T denoting the Boltzmann constant and temperature, respectively. l_B is the Bjerrum length in a units, E_C is the electrostatic potential of the pair of ions at contact, and the reduced temperature T^* is in units of E_C. The unit step function $\theta(x) = 1$ for $x > 0$ and $\theta(x) = 0$ for $x < 0$ prevents contributions to the electrostatic energy of the pair of ions that would come from forbidden overlap of the hard cores. We introduce the notation $V_{++}^{C} = V_{--}^{C} = V^{C} = -V_{+-}^{C}$.

We limit ourselves to systems with anions and cations with different chemical natures, where the SR cross-interactions are significantly weaker than the SR interactions between ions of the same sign. Based on this assumption, in our approximate theory the SR interactions between the anions and the cations are neglected. For $V_{ii}^{A}(r)$ we assume a short-range attractive potential. The form of the sum of the direct (van der Waals type) and solvent-induced interactions is unknown, but we assume that its detailed shape is not necessary for studies of the collective phenomena such as the long-distance correlations. For simplicity of calculations, we assume the attractive Yukawa potentials,

$$\beta V_{ii}^{A}(r^*) = -l_B\varepsilon_{ii}^*\frac{e^{-\alpha_i^*(r^*-1)}}{r^*}\theta(r^*-1), \quad i = +,-, \tag{5}$$

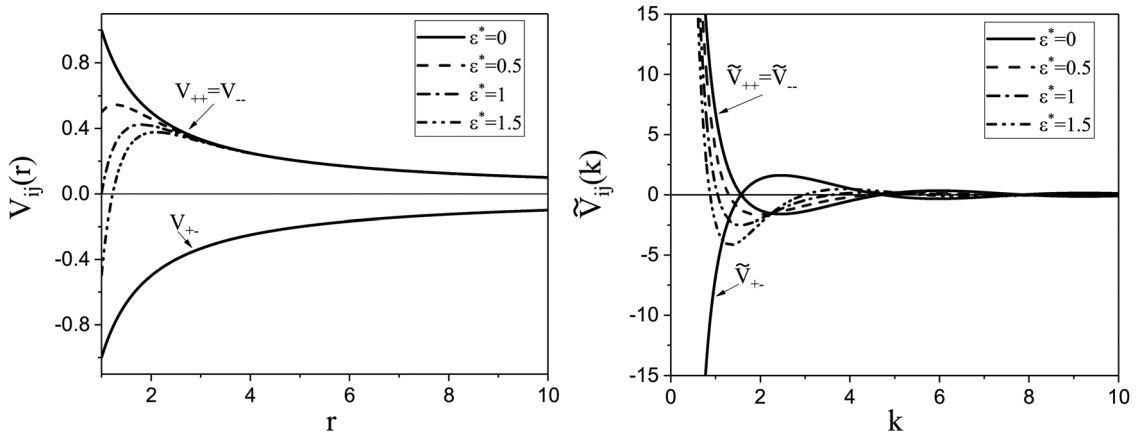

Fig. 1 The interaction potentials $V_{ij}(r)$ for the model with $\varepsilon^* = 0$, 0.5, 1, and 1.5 in real space (a) and in Fourier representation (b). V_{ij} are in units of E_C. r and k are in a and a^{-1} units, respectively.

where α_i^* has units of a^{-1}, and we assume that $\alpha_+^* = \alpha_-^* = \alpha = 1.8$ to assure fast decay of these interactions. $\varepsilon_{ii}^* = \varepsilon_{ii}/E_C$ measures the strength of the effective non-Coulomb interactions in units of E_C and we assume $\varepsilon_{++}^* = \varepsilon_{--}^* = \varepsilon^*$. Then, $V_{++}^A = V_{--}^A = V^A$. The interaction potentials $V_{++}(r) = V_{--}(r)$ and $V_{+-}(r)$, and their Fourier transforms are shown in Fig. 1 for $0 \le \varepsilon^* \le 1.5$, where the explicit expressions for $\tilde{V}^C(k)$ and $\tilde{V}^A(k)$ are

$$\beta\tilde{V}^C(k) = 4\pi l_B \frac{\cos k}{k^2} \tag{6}$$

and

$$\beta\tilde{V}^A(k) = -4\pi l_B \varepsilon^* \frac{\cos k + \alpha \sin k/k}{\alpha^2 + k^2}. \tag{7}$$

Note that $\beta\tilde{V}^C(k)$ and $\beta\tilde{V}^A(k)$ take the minimum at $k = 2.46$[7] and at $k = 0$, respectively.

According to ref. 27–29, the strength of the van der Waals interactions in various systems is in the range $0–10k_BT$. Based on the literature data,[25] we expect that the physically relevant strength of the SR interactions in our E_C units is $0 \le \varepsilon^* \le 1$.

B. Approximate theory for the structure in the absence of boundaries

In this section, we briefly summarize the mesoscopic density functional theory,[7] fix the notation, and present results for the structure in the bulk for the model presented in Section II A. The theory is based on the assumption that the density and charge of each ion are both uniformly distributed over the hard core. Local volume fractions $\pi\rho_i(\mathbf{r})/6$ in regions of linear size a around $\mathbf{r}$ are equal to the fraction of the volume of the considered region that is occupied by the cores of the i-th type ions. $\rho_i(\mathbf{r})$ denotes the corresponding dimensionless density. By this construction, continuous functions are obtained for each microscopic configuration. Because of the symmetry of the assumed interaction potentials, it is convenient to change the variables to the dimensionless charge and number density of ions,

$$c(\mathbf{r}) = \rho_+(\mathbf{r}) - \rho_-(\mathbf{r}), \quad \rho(\mathbf{r}) = \rho_+(\mathbf{r}) + \rho_-(\mathbf{r}).$$

For the electrostatic properties such as the capacitance, the local charge density $c(\mathbf{r})$ plays the key role.

The average charge in a region of the linear size $\sim a$ vanishes in the absence of boundaries or external fields because the probability that the considered region is occupied by a positively or negatively charged ion is the same. In dilute electrolytes, the considered region is most probably occupied by the solvent and the most probable and average local charge are both equal to zero. In contrast, in concentrated ionic systems such as ionic liquids, the most probable and average charge in the region of the linear size $\sim a$ is significantly different, because for a very small density of the solvent this region is most probably occupied by either an anion or a cation. Moreover, in the most probable configurations the nearest neighbors are oppositely charged, because in this case the electrostatic energy is minimized. Thus, the dominant fluctuations of the local charge, $\phi(\mathbf{r})$, have a form of charge waves and should be taken into account. Since $\langle\phi(\mathbf{r})\rangle = 0$, the appropriate measure of such fluctuations is the variance $\langle\phi(\mathbf{r})^2\rangle$ of the local charge in a region of the linear size $\sim a$. In the bulk this variance is independent of the position. To highlight the significance of the charge fluctuations in concentrated ionic systems, we illustrate schematically the qualitative shape of the probability of the local deviation of the charge from the average value (zero in the bulk) in Fig. 2.

In the theory developed in ref. 7 and 9, the grand potential functional of $c(\mathbf{r})$ and $\rho(\mathbf{r})$ is split in two parts, one with frozen mesoscopic fluctuations, *i.e.* of the mean-field (MF) type and denoted by Ω_{co}, and the other one containing the fluctuation contribution and denoted by Ω_{fl},

$$\beta\Omega[c, \rho] = \beta\Omega_{co}[c, \rho] + \beta\Omega_{fl}[c, \rho], \tag{8}$$

where $c(\mathbf{r})$ and $\rho(\mathbf{r})$ play the role of constraints imposed on microscopic states. We study electrostatic properties in the ion-rich phase under thermodynamic conditions far from the critical region; therefore in the present theory we neglect fluctuations of ρ playing an important role only close to the critical point. We take into account the dominant charge–density fluctuations

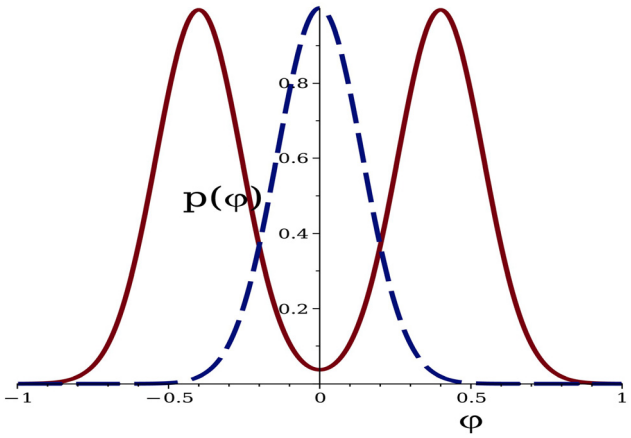

Fig. 2 Schematic illustration of the type of the probability $p(\phi)$ of the deviation ϕ of the charge from the average value in regions of the linear size $\sim a$ for dilute electrolytes (dashed blue line) and for ionic liquids (continuous red line). The average charge vanishes in the two cases, but in the case of concentrated ionic systems, fluctuations of the charge in regions of the linear size $\sim a$ are large and should be taken into account.

with the period $\sim 2a$ and make the approximation consistent with statistical–mechanical definition of the grand thermodynamic potential,

$$\beta\Omega_{\mathrm{fl}}[c,\rho] = -\ln\int D\phi\,\exp[-(\beta\Omega_{\mathrm{co}}[c+\phi,\rho]-\beta\Omega_{\mathrm{co}}[c,\rho])]. \quad (9)$$

The functional integral in the above equation is over the deviations $\phi(\mathbf{r})$ of the local charge from the field $c(\mathbf{r})$.

On the level of the self-consistent Gaussian approximation, we assume that in eqn (9)

$$\beta\Omega_{\mathrm{co}}[c+\phi,\rho]-\beta\Omega_{\mathrm{co}}[c,\rho] \approx \frac{1}{2}\int \mathrm{d}\mathbf{k}\tilde{\phi}(\mathbf{k})\tilde{C}_{\mathrm{cc}}(k)\tilde{\phi}(-\mathbf{k}), \quad (10)$$

where $1/\tilde{C}_{\mathrm{cc}}(k)$ is the charge–charge correlation function in Fourier representation and

$$\tilde{C}_{\mathrm{cc}}(k) = \frac{\delta^2\beta\Omega[c,\rho]}{\delta\tilde{c}(\mathbf{k})\delta\tilde{c}(-\mathbf{k})}. \quad (11)$$

In the self-consistent Gaussian approximation (effectively one-loop approximation in the field theory) eqn (8)–(11) should be solved self-consistently. Note that for Ω given in (8), the inverse correlation function contains a fluctuation contribution coming from $\beta\Omega_{\mathrm{fl}}$. The development of the theory and further technical details can be found in ref. 7.

For the model discussed in Section II A, the grand thermodynamic potential functional in the presence of the mesoscopic constraints (frozen mesoscopic fluctuations) can be written in the form

$$\beta\Omega_{\mathrm{co}}[c,\rho] = \beta U^{c}_{\mathrm{co}}[c] + \beta U^{\rho}_{\mathrm{co}}[\rho] + \int \mathrm{d}\mathbf{r}\beta f_{\mathrm{h}}(c,\rho) - \beta\mu\int \mathrm{d}\mathbf{r}\rho(\mathbf{r}),$$

where μ is the chemical potential of the ions, and the contributions to the internal energy are given by

$$\beta U^{c}_{\mathrm{co}}[c] = \frac{1}{2}\int \mathrm{d}\mathbf{r}_1\int \mathrm{d}\mathbf{r}c(\mathbf{r}_1)\beta V_{\mathrm{cc}}(r)c(\mathbf{r}_1+\mathbf{r})$$
$$= \frac{1}{2}\int \mathrm{d}\mathbf{k}\tilde{c}(\mathbf{k})\beta\tilde{V}_{\mathrm{cc}}(k)\tilde{c}(-\mathbf{k})$$

and

$$\beta U^{\rho}_{\mathrm{co}}[\rho] = \frac{1}{2}\int \mathrm{d}\mathbf{r}_1\int \mathrm{d}\mathbf{r}\rho(\mathbf{r}_1)\beta V_{\rho\rho}(r)\rho(\mathbf{r}_1+\mathbf{r})$$
$$= \frac{1}{2}\int \mathrm{d}\mathbf{k}\tilde{\rho}(\mathbf{k})\beta\tilde{V}_{\rho\rho}(k)\tilde{\rho}(-\mathbf{k}),$$

with $\tilde{V}_{\mathrm{cc}}(k)$ and $\tilde{V}_{\rho\rho}(k)$ having the form:

$$\tilde{V}_{\mathrm{cc}}(k) = \tilde{V}^{\mathrm{C}}(k) + \frac{1}{2}\tilde{V}^{\mathrm{A}}(k), \quad \tilde{V}_{\rho\rho}(k) = \frac{1}{2}\tilde{V}^{\mathrm{A}}(k), \quad (12)$$

where $\tilde{V}^{C}(k)$ and $\tilde{V}^{A}(k)$ are given in (6) and (7). For simplicity of notation, we omit the asterisks and from now on r and k are in a and $1/a$ units, respectively. The Fourier transforms $\tilde{V}_{\mathrm{cc}}(k)$ and $\tilde{V}_{\rho\rho}(k)$ are presented in Fig. 3. Because the hard cores of the ions cannot overlap, in our theory the largest wavenumber of the charge wave in a^{-1} units is $k_{\max} = \pi$, since the smallest wavelength of the charge wave corresponds to a pair of oppositely charged ions at contact. Note the minima of $\tilde{V}_{\mathrm{cc}}(k)$ and $\tilde{V}_{\rho\rho}(k)$ at $k = k_0 > 0$ and $k = 0$, respectively.

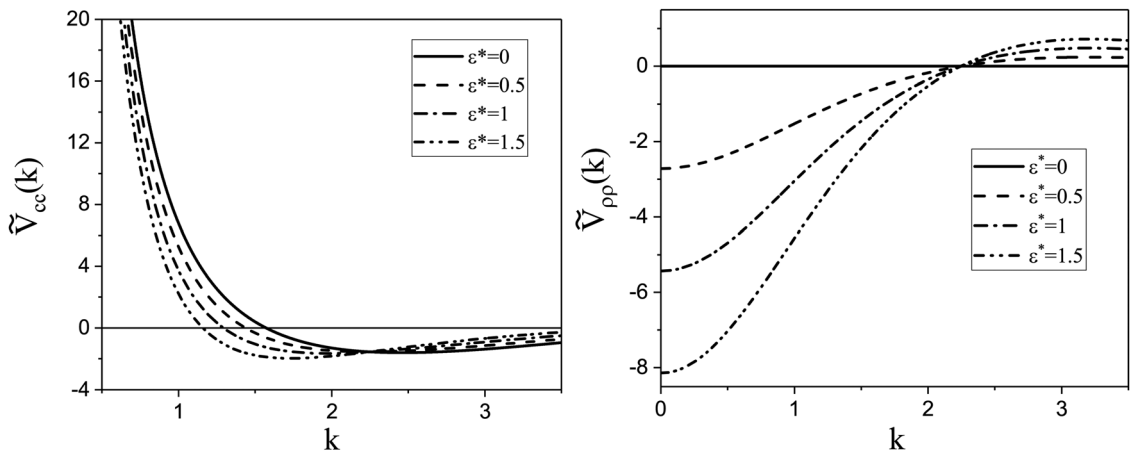

Fig. 3 The Fourier transforms $\tilde{V}_{\mathrm{cc}}(k)$ and $\tilde{V}_{\rho\rho}(k)$ for the model with $\varepsilon^* = 0$, 0.5, 1, and 1.5.

$f_h(c(\mathbf{r}), \rho(\mathbf{r}))$ is the free-energy density of the hard-core reference system,

$$\beta f_h = \rho_+ \ln \rho_+ + \rho_- \ln \rho_- + \beta f_{hs}[\rho], \tag{13}$$

where the first two terms come from the entropy of mixing, and $f_{hs}[\rho]$ is the contribution to the free energy density associated with packing of hard spheres with diameter a. The form of f_{hs} is independent of the charge density $c(\mathbf{r})$, and the ion-poor–ion-rich phase transition is induced by long-wavelength fluctuations, $\tilde{\rho}(k)$ for $k \to 0$. For the above reasons, for determination of the electrostatic properties and the phase separation between ion-poor and ion-rich phases, the local-density approximation can be applied, and we assume for $f_{hs}(\rho)$ the Carnahan–Starling approximation.[30]

The theory summarized above allows calculation of the correlation functions. The second functional derivative of $\beta\Omega$ with respect to c is[7]

$$\tilde{C}_{cc}(k) = \beta \tilde{V}_{cc}(k) + \frac{1}{\rho_R} \tag{14}$$

where $\tilde{V}_{cc}(k)$ takes a negative minimum for $k = k_0 > 0$ (see Fig. 3), and

$$\frac{1}{\rho_R} = \frac{1}{\rho} + \frac{\langle \phi^2 \rangle}{\rho^3}. \tag{15}$$

The last term in (15) is the fluctuation contribution. The dominant fluctuations are the charge waves with the wavenumber k_0 that can be interpreted as the formation of chains of alternating anions and cations. As a result of these fluctuations (formation of charge–neutral aggregates), $\rho_R < \rho$ can be interpreted as the density of free ions. Note that in our approach, the smaller effective density of ions plays a role analogous to the smaller effective charge of 'dressed ion' in the Kjellander theory,[31,32] since both lead to a decrease of the effective charge in small regions. This also establishes some link with the theories applying the concept of ion association.[33–37] According to this concept, an electrolyte solution is considered as a mixture of free ions and ionic clusters in chemical equilibrium, whereas in our theory the reduction of free ions arises as a result of accounting for charge–charge correlations.

For $k \approx k_0$ eqn (14) takes the approximate form[7]

$$\tilde{C}_{cc}(k) \approx \tilde{C}_a(k) = \beta \tilde{V}_{cc}(k_0) + \beta v\left(k^2 - k_0^2\right)^2 + \frac{1}{\rho_R}, \tag{16}$$

where we take into account that $\tilde{C}_{cc}(k)$ is an even function of k. In this approximation, the variance of the local charge density is given by ref. 7 and 9

$$\langle \phi^2 \rangle \approx \int \frac{d\mathbf{k}}{(2\pi)^3} \tilde{C}_a^{-1}(k) = \frac{k_0}{4\pi\sqrt{\tilde{C}_a(k_0)\beta v}}, \tag{17}$$

and the self-consistent solution of (14)–(17) can be obtained analytically. Eqn (16) is a reasonably good approximation for $\tilde{C}_{cc}(k)$ when $l_B\rho > 1$, as already discussed in ref. 7 for the pure RPM. For small $l_B\rho$, the approximation (16) is valid for too small regions of k, and the inverse Fourier transform of $\tilde{C}_a(k)^{-1}$ to the real space gives the wrong results.[7,11] In this work, however, we limit ourselves to a large density of ions at relatively low T^*, *i.e.* to the ion-rich phase, where the approximation $\tilde{C}_{cc}(k) \approx \tilde{C}_a(k)$ is valid on a semiquantitative level as will be shown in Section III.

The SR interactions may induce macroscopic phase separation into ion-poor–ion-rich phases. As we are interested in the double-layer capacitance in the ion-rich phase, we should make sure that the considered thermodynamic parameters do not correspond to a two-phase region. To estimate the range of T^* and ρ corresponding to the one-phase region, we determine the instability with respect to the gas–liquid type of phase separation in the MF approximation. The MF spinodal is given by $\tilde{C}^{MF}_{\rho\rho}(0) = 0$, where

$$\tilde{C}^{MF}_{\rho\rho}(k) = \frac{\delta^2 \beta\Omega_{co}[c, \rho]}{\delta\tilde{\rho}(\mathbf{k})\delta\tilde{\rho}(-\mathbf{k})} = \beta \tilde{V}_{\rho\rho}(k) + \frac{d^2 \beta f_h(\rho)}{d\rho^2}. \tag{18}$$

C. Approximate theory for a semi-infinite system

In this section we derive the Euler–Lagrange (EL) equation for the charge density near the electrode for the RPM+SR model introduced in Section II A, using the mesoscopic theory presented in Section II B. Following ref. 11, we assume that the charge of the electrode belongs to the system. We also assume that c and ρ depend only on the distance from the electrode. In the case of lateral inhomogeneity, one should consider c and ρ averaged over the planes parallel to the electrode, as done in ref. 38. The system as a whole is charge neutral, and contains the whole charge of the electrode and of the ionic solution, meaning that $c(z) = 0$ for $z < 0$. As in ref. 11, we assume that the charge of the electrode is accumulated on its flat surface. In our theory, $\pi\rho_i(z)/6$ is the fraction of the volume of the layer with the mid-plane at z and a thickness a that is covered by the i-th type ions. Because of that, we chose $z = 0$ inside the electrode, at the distance $a/2$ from its surface. For this choice of $z = 0$, we ensure that a layer with a center at $z < 0$ contains contributions neither from the charge localized at the surface of the electrode nor from the charge of the ions in the liquid. As a result, the charge neutrality condition takes the simple form $\int_0^\infty c(z)dz = 0$. The system is illustrated in Fig. 4.

In the presence of the electrode, the equilibrium distribution of the ions is determined by the minimum of the excess grand potential

$$\Delta\beta\Omega[\bar{\rho}; c, \Delta\rho] = \beta\Omega[c, \bar{\rho} + \Delta\rho] - \beta\Omega[0, \bar{\rho}] + \beta U_{wall},$$

where $\bar{\rho}$ and $\bar{c} = 0$ are the dimensionless density and charge of the ions in the bulk, respectively, and $\Delta\rho(z)$ and $c(z)$ are the dimensionless excess density and charge at the distance z from the system boundary. βU_{wall} is the contribution to the grand potential associated with direct SR interactions between the ions and the electrode, and has the form

$$\beta U_{wall}/A = \int_0^\infty dz\left[\rho_+(z)h_+(z) + \rho_-(z)h_-(z)\right] = \int_0^\infty dz c(z)h(z) + \cdots,$$

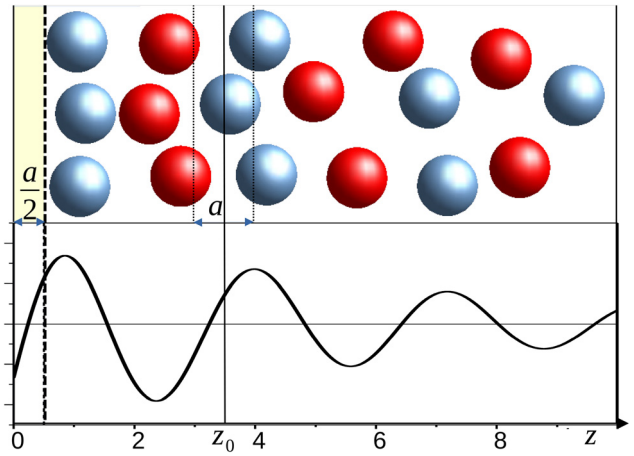

Fig. 4 Top: Cartoon with a particular distribution of ions with positive (blue) and negative (red) charges near an electrode. The yellow region is the part of the electrode included in the considered system with $z \geq 0$. The surface of the electrode is indicated by the dashed line. Bottom: An example of the dimensionless charge density $c(z) = \rho_+(z) - \rho_-(z)$, with z in units of the ion diameter a. In the mesoscopic theory, $\pi\rho_i(z_0)/6$ is the fraction of the volume between the surfaces indicated by the dotted lines in the cartoon above the plot that is covered by the i-th type ions. Note that $\rho_i(z_0)$ depends on the distribution of the i-th type ions in the vicinity of the plane at $z = z_0$. The dimensionless charge of the electrode in this mesoscopic theory is $Q_e = \int_0^{1/2} c(z)\mathrm{d}z$.

where A is the electrode surface, $h_+(z)$ and $h_-(z)$ describe interactions with the uncharged electrode of the cations and the anions, respectively, $h(z) = (h_+(z) - h_-(z))/2$, and the dots refer to the contribution depending on $\Delta\rho$ that is not relevant for the electrostatic properties. The form of $h_\pm(z)$ strongly depends on the chemical nature of the ions and the electrode,[27,28,39] but in general both $h_+(z)$ and $h_-(z)$ are of a short range. In systems where preferential adsorption of either the anions or the cations at the uncharged electrode takes place, the ranges and amplitudes of $h_+(z)$ and $h_-(z)$ are not the same. Since the plane with $z = 0$ is located inside the electrode, in our model $h_\pm(z) \to 0$ for $z \to 0$.

For small voltage and weak surface selectivity, $c(z)$ and $\Delta\rho(z)$ are small, and we can Taylor expand $\beta\Omega[c,\bar{\rho} + \Delta\rho] - \beta\Omega[0,\bar{\rho}]$ in terms of $c(z)$ and $\Delta\rho(z)$. For $\bar{\rho}$ and $\bar{c} = 0$ corresponding to the equilibrium in the bulk, the first functional derivatives vanish, and the lowest-order term in the Taylor expansion is of second order in the fields $c(z)$ and $\Delta\rho(z)$. In Fourier representation, the second functional derivatives are given by $\tilde{C}_{cc}(k)$ and $\tilde{C}_{\rho\rho}(k)$ (see Section II B). For concentrated ionic solutions, we chose the approximation $\tilde{C}_{cc}(k) \approx \tilde{C}_a(k)$ (see eqn (16)), as previously done for the RPM in ref. 38. Returning from the Fourier to the real-space representation and performing the standard minimization procedure, we obtain the following EL equation for the equilibrium charge distribution

$$\left(A_0 + A_2\frac{d^2}{dz^2} + A_4\frac{d^4}{dz^4}\right)c(z) + h(z) = 0, \tag{19}$$

where

$$A_0 = \tilde{C}_a(k_0) + \beta\nu k_0^4 \tag{20}$$

$$A_2 = 2\beta\nu k_0^2 \tag{21}$$

$$A_4 = \beta\nu \tag{22}$$

refer to the expansion of $\tilde{C}_{cc}(k)$ about $k = k_0$, *i.e.* to $\tilde{C}_a(k)$ (see (16)). For more details concerning derivation of (19) in the case of pure RPM see ref. 11 and 38. In our model k_0, $\tilde{C}_a(k_0)$ and $\beta\nu$ depend on both the Coulomb and the SR interactions (see (6), (7) and (12)), and on $l_B = 1/T^*$. $\tilde{C}_a(k_0)$ depends in addition on ρ_R.

III. Results and discussion

In this section, we first focus on the phase separation and the structure of the ion-rich phase. Next, we redefine the capacitance in the present mesoscopic formalism using an alternative definition of the charge of the electrode, and show that the new definition gives much better results for the RPM than the one used in ref. 11. We use this new definition of the charge in the present model, and obtain formulas for the PZC and the capacitance in the presence of the specific interactions.

A. Bulk properties of the RPM+SR model

For the model (2)–(5), the resulting equation for the MF gas–liquid type spinodal, $\tilde{C}^{MF}_{\rho\rho}(0) = 0$, has the explicit form:

$$T^* = \frac{2\pi\varepsilon^*(1+\alpha)}{\alpha^2\dfrac{\partial^2\beta f_h}{\partial\rho^2}}, \tag{23}$$

and the spinodal line is shown in Fig. 5 for $\alpha = 1.8$ and $\varepsilon^* = 0.5$, 1, 1.5. Since the region unstable with respect to the phase separation is overestimated in MF, we can safely choose $\rho = 0.8$ and $T^* = 0.5$ for further consideration.

The critical temperature (maximum of T^* at the spinodal) increases linearly with the strength ε^* of the SR interactions. We compared our result with the experimentally obtained critical temperature for an aqueous system of imidazolium-based ionic liquids,[25] and verified that the physically relevant strength of the SR interactions in E_C units is $\varepsilon^* \sim 1$. For the estimation of the order of magnitude of ε^* for an aqueous system of imidazolium-based ionic liquids see the Appendix.

The structure factor of the charge–charge correlations, $S(k) = \tilde{C}_{cc}(k)^{-1}/\rho$, is shown in Fig. 5 for $\rho = 0.8$, $T^* = 0.5$ and $\varepsilon^* = 1$. The agreement between $\tilde{C}_{cc}(k)$ (eqn (14)) and the approximation $\tilde{C}_a(k)$ (eqn (16)) is satisfactory on the semiquantitative level, and we shall use the approximate analytical theory based on $\tilde{C}_a(k)$ in studies of the capacitance.

The SR interactions in Fourier representation, $\tilde{V}_A(k)$, take the minimum for $k = 0$, therefore with increasing amplitude ε^* of these interactions, the minimum of $\tilde{V}_{cc}(k) = \tilde{V}_C(k) + \tilde{V}_A(k)/2$ moves to smaller k. The period, $2\pi/\alpha_1 \approx 2\pi/k_0$, and the range α_0^{-1} of the oscillatory decay of the charge–charge correlations both increase monotonically with increasing strength of the SR attraction between ions with the same charge. $\tilde{V}_{cc}(k_0)$ is a nonmonotonic function of ε^* as a result of competition between $\tilde{V}_C(k)$ and $\tilde{V}_A(k)$ for k between the minimum of $\tilde{V}_C(k)$ and the minimum of $\tilde{V}_A(k)$. In Fig. 6, the energy gain $\tilde{V}_{cc}(k_0)$ associated with the dominating charge waves, the

corresponding wavenumber k_0, the correlation length of the charge–charge correlations, $1/\varkappa_0$, as well as the density ρ_R of 'free' ions, are shown for $\tilde{C}_{cc}(k)$ approximated by $\tilde{C}_a(k)$ (see (16)). $\varkappa_0$ is given by an analytic expression (see the Appendix).

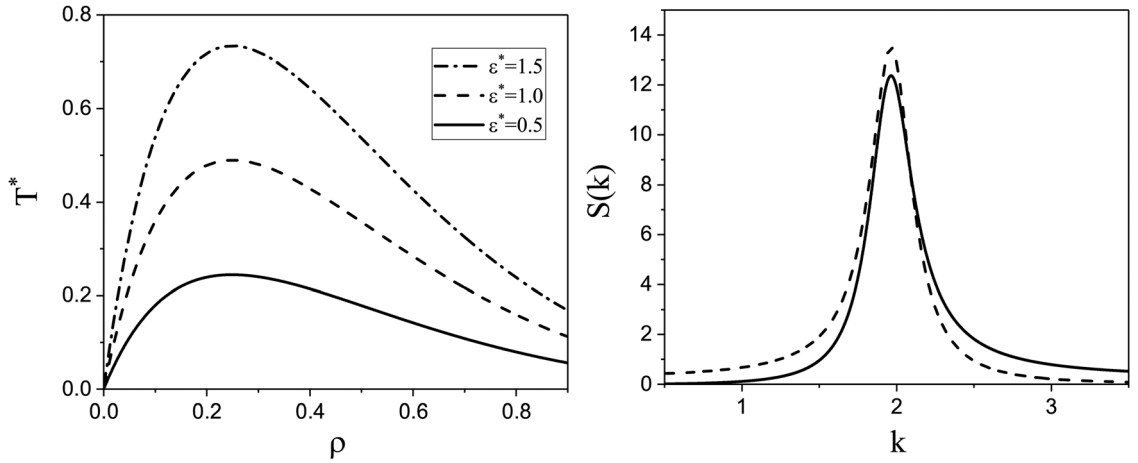

Fig. 5 Left: The spinodal line of the phase separation into ion-poor–ion-rich phases for the model with $\varepsilon^* = 0.5$, 1, and 1.5. Charge fluctuations are taken into account in the self-consistent Gaussian approximation, and the fluctuations of ρ are neglected (see Section II B), so that the presented spinodal lines are on the MF level with respect to ρ. Right: Structure factor $S(k) = \tilde{C}_{cc}(k)^{-1}/\rho$ for the charge–charge correlations for $\rho = 0.8$, $T^* = 0.5$ and $\varepsilon^* = 1$ in the self-consistent Gaussian approximation. Solid and dashed lines denote the structure factor for $\tilde{C}_{cc}(k)$ given in eqn (14), and for the approximation $\tilde{C}_a(k)$ given in eqn (16), respectively. k is in a^{-1} units. $T^* = k_B T/E_C$ and ε^* is the SR interaction between like ions in units of $E_C = e^2/(a\epsilon)$.

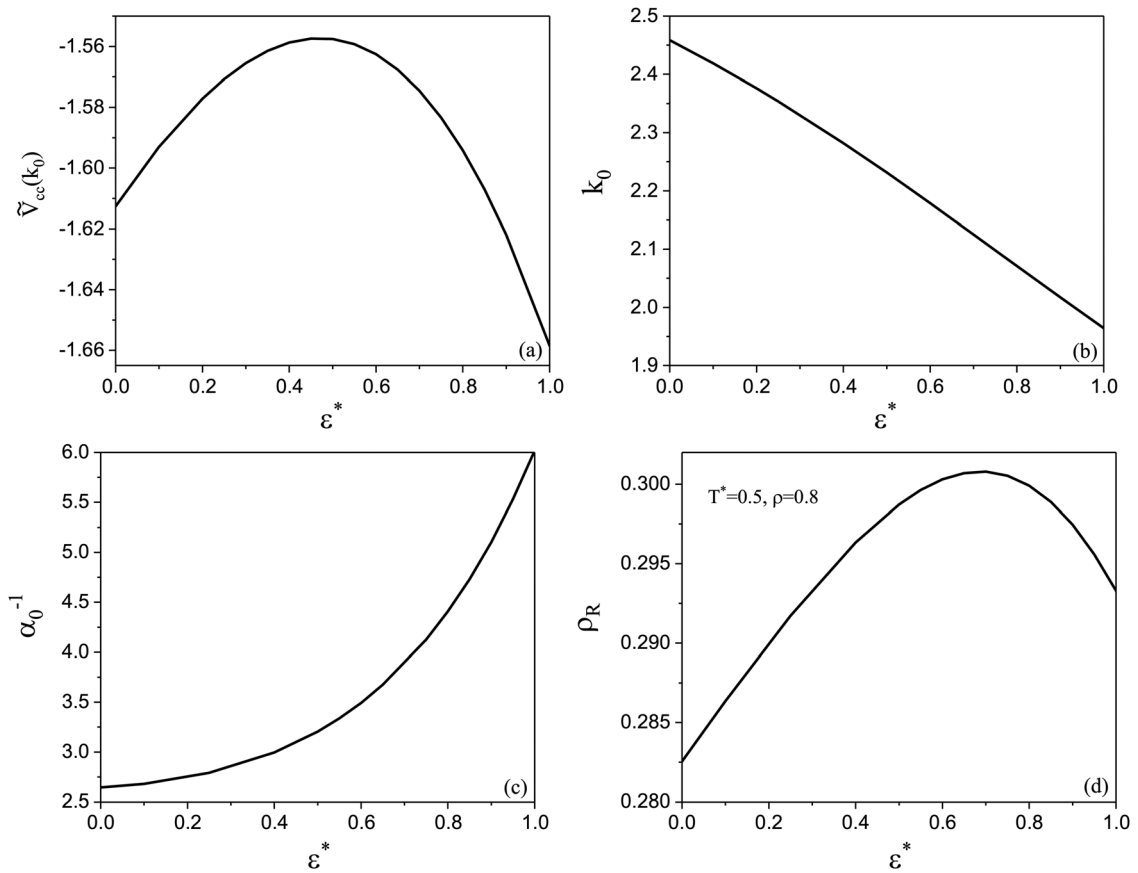

Fig. 6 (a) The minimum of the interaction potential $\tilde{V}_{cc}(k)$ (see (12)), (b) the wavenumber of the most probable charge waves $k_0 \approx \varkappa_1$, (c) the charge–charge correlation length $\varkappa_0^{-1}$ and (d) the renormalized dimensionless density of ions ρ_R (eqn (15)) related to 'free' ions in the self-consistent Gaussian approximation, for $T^* = 0.5$ and $\rho = 0.8$. $\tilde{V}_{cc}$ and the strength of the SR interactions between ions of the same sign, ε^*, are in E_C units, k_0 and $\varkappa_0$ are in $1/a$ units, and ρ_R is dimensionless.

The variance of the local charge, $\langle\phi^2\rangle$ (related to the amplitude of the charge wave) takes a minimum for $\varepsilon^* \approx 0.7$ corresponding to $k_0 \approx 2.1$ for which the average thickness of the alternating charged layers, π/k_0, is very close to 1.5 (in a units). It corresponds to a crossover from alternating charged monolayers to alternating charged bilayers, *i.e.* to weaker charge ordering in instantaneous states. The minimum of $\langle\phi^2\rangle$ corresponds to the maximum of the renormalized density of ions, ρ_R (see eqn (15)), related to the density of 'free' ions in the concentrated system. This means that when the ordering into charge waves (charge–neutral aggregates in real space) becomes weaker and $\langle\phi^2\rangle$ takes a minimum, then more 'free' ions are present in the system.

B. Capacitance in the pure RPM with the new definition of the charge at the electrode

The linear eqn (19) can be solved rather easily for fixed $c(0)$ and under the charge-neutrality condition $\int_0^\infty c(z)\mathrm{d}z = 0$. When $c(z)$ is known, we can obtain the electrostatic potential from the formula

$$\Psi(z) = \frac{4\pi e}{a}\int_z^\infty \mathrm{d}z'(z-z')c(z'), \tag{24}$$

and the capacitance is given by

$$C = \frac{eQ_e/a^2}{\Psi(0)},$$

where e is the elementary charge and eQ_e/a^2 is the charge of the electrode per unit area. We limit ourselves to small voltages, so that the linearized EL eqn (19) is a fair approximation in the ion-rich phase.

In ref. 11 limited to pure RPM, the solution of the more general linearized EL equation (based on $\tilde{C}_{cc}(k)$ rather than on $\tilde{C}_a(k)$) was obtained and the charge at the electrode per unit area was identified with $e\sigma_0 = ec(0)/a^2$. For small and large ρ, a monotonic and an oscillatory asymptotic decay of $c(z)$ for $z \to \infty$ was obtained, respectively. The two cases are separated by the Kirkwood line[3,40] on the (ρ, T) plane. The obtained capacitance was overestimated in both cases, and we speculated that the missing factor $f \sim 1/3$ was associated with the microscopic structure near the electrode that is not accurately determined in the mesoscopic theory.

Let us return to the question of the charge at the electrode. Within our mesoscopic theory, the dimensionless charge inside a layer between $z = z_0$ and $z = z_1$ is given by $Q = \int_{z_0}^{z_1} c(z)\mathrm{d}z$. Consistent with the construction of the theory, where the surface of the electrode is at $z = 1/2$ (in a units), the dimensionless charge of the electrode should be given by

$$Q_e = \int_0^{1/2} c(z)\mathrm{d}z. \tag{25}$$

In the following, we verify if with this definition of Q_e, a better agreement with the Debye capacitance for dilute electrolytes and with simulation results for concentrated electrolytes is obtained for the pure RPM.

The charge density on the small-density side of the Kirkwood line in this theory has the form[11]

$$c(z) = \frac{c(0)\left(\mathrm{e}^{-a_1 z} - \frac{a_2}{a_1}\mathrm{e}^{-a_2 z}\right)}{1-\frac{a_2}{a_1}},$$

where $a_1 > a_2$. From the above and (25) we obtain

$$Q_e = \frac{c(0)(1-\delta)}{a_1\left(1-\frac{a_2}{a_1}\right)},$$

where $\delta = 1 - \mathrm{e}^{-a_2/2} + \mathrm{e}^{-a_1/2}$. For $a_1 > 3$, $a_2 \ll 1$, which is the case for dilute electrolytes,[3,41] $\delta \simeq a_2/2 + \mathrm{e}^{-a_1/2} \ll 1$. The capacitance takes the form

$$C = \frac{eQ_e/a^2}{\Psi(0)} = \frac{\epsilon a_2(1-\delta)}{4\pi a\left(1-\frac{a_2}{a_1}\right)} \simeq \frac{\epsilon a_2}{4\pi a} \simeq \frac{\epsilon}{4\pi\lambda_D},$$

where the first approximate equality holds for $a_2/a_1 \ll 1$, $\delta \ll 1$, and the last one follows from $a_2 \approx a/\lambda_D$, as shown in ref. 11 for $\rho \to 0$. We should note that in the DH theory, $a_1 = \infty$, and only a single exponential term remains. With the present definition of the charge at the electrode, our theory reduces precisely to the DH theory for dilute electrolytes.

On the large-density side of the Kirkwood line, $c(z)$ decays in an oscillatory way,

$$c(z) = \frac{c(0)}{\sin(\theta)}\sin(\alpha_1 z + \theta)\exp(-\alpha_0 z)$$

and after inserting the above into eqn (25) and (24), we obtain $Q_e = c(0)f$ and

$$C = \frac{\epsilon\left(\alpha_0^2 + \alpha_1^2\right)}{4\pi a}f, \tag{26}$$

where the factor resulting from the mesoscopic charge distribution at the electrode is

$$f = \frac{\sin(\alpha_1/2)\exp(-\alpha_0/2)}{\alpha_1}. \tag{27}$$

Since $0 \le \alpha_1 \le \pi$, we have $\frac{1}{\pi}\exp(-\alpha_0/2) \le f \le \frac{1}{2}\exp(-\alpha_0/2)$. For the parameters $\alpha_1 \approx 2.45$, $\alpha_0 \approx 0.118$ corresponding to the conditions assumed in the simulations of ref. 12, we obtain neglecting f in (26) $C \approx 0.5$,[11] whereas in the simulations the result was $C_{sim} \approx 0.15$. Eqn (27) gives for $\alpha_1 \approx 2.45$, $\alpha_0 \approx 0.118$ the result $f \approx 0.36$, and from (26) we obtain $C \approx 0.18$, which agrees much better with the simulations.

The above results for dilute and concentrated electrolytes confirm that if in our mesoscopic theory the charge at the electrode is given by the formula (25), then much more accurate expression for the capacitance is obtained. We shall use (25) for the capacitance and the PZC in the RPM+SR system.

C Capacitance at the PZC in the presence of short-range specific interactions – the case of the ion-rich phase

Here we first consider a selective electrode with the specific electrode–ion interactions that are of a short range, but otherwise are of an arbitrary form. Next, we illustrate our results on a particular example of the potential $h(z)$.

The solution of eqn (19) for the RPM+SR model in the presence of the selective electrode has the form

$$c(z) = c_0(z) + \Delta c(z) \tag{28}$$

where

$$c_0(z) = \frac{A}{\sin\theta} e^{-\alpha_0 z} \sin(\alpha_1 z + \theta) \tag{29}$$

satisfies the EL eqn (19) for $h(z) = 0$, and $\Delta c(z)$ is the solution that has a short range determined by the form of $h(z)$. We assume that the functions I_i defined by

$$I_i(z) - I_i(0) = \int_0^z z'^{(i-1)} \Delta c(z') \mathrm{d}z'$$

and relevant for $\Psi(0)$ and Q_e, satisfy $\lim_{z\to\infty} I_i(z) = 0$ for $i = 1, 2$.

The amplitude and phase in (29) are determined by the charge-neutrality condition, $\int_0^\infty c_0(z)\mathrm{d}z = I_1(0)$, and by the value Q_e of the charge at the electrode (see (25)), and depend on the form of Δc through $I_1(0)$ and $I_1(1/2)$. The corresponding equations for θ and A are given in the Appendix.

The electrostatic potential at $z = 0$ for the considered form of $c(z)$ can be obtained from (24). Using (24) and (29) and the expressions for $\cot\theta$ and A given in the Appendix, we obtain

$$\Psi(0) = \frac{4\pi e}{\epsilon a} \frac{Q_e}{(\alpha_0^2 + \alpha_1^2) f} + \Psi_{PZC}$$

where f is given in (27), and where

$$\Psi_{PZC} = \frac{4\pi e}{\epsilon a}\left[I_2(0) + \frac{I_1(0) P e^{-\alpha_0/2} - I_1(1/2)}{(\alpha_0^2 + \alpha_1^2) f} \right]$$

with

$$P = \cos(\alpha_1/2) - \frac{\alpha_0}{\alpha_1}\sin(\alpha_1/2)$$

which is identified with the PZC.

The capacitance at the PZC,

$$C = \frac{eQ_e/a^2}{\Psi(0) - \Psi_{PZC}},$$

is given by eqn (26), *i.e.* by the same formula as in the RPM, and depends only on , a, α_0 and α_1. The inverse lengths α_0 and $\alpha_1 \approx k_0$ characterize the bulk structure and depend on ε^*, as shown in Fig. 6. Thus, C is independent of the specific electrode–ion interactions, and as a function of ε^* is shown in Fig. 7. We obtain almost linear decrease of C/C_H with increasing ε^*. The attractive SR interactions between the ions with the same charge compete with the repulsive Coulomb potential, and lead to a larger period and larger decay length of the oscillatory decay of $c(z)$.

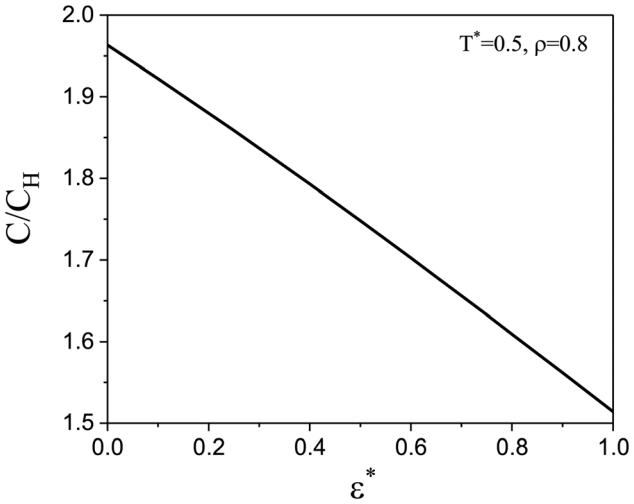

Fig. 7 The capacitance C at the PZC in units of the Helmholtz capacitance $C_H = \epsilon/(4\pi a)$. $T^* = 1/l_B = 0.5$, and $\rho = 0.8$. The strength of the specific ion–ion interaction ε^* is in E_C units.

To illustrate our result for Ψ_{PZC} on a particular example, we consider an uncharged electrode adsorbing anions and assume

$$h(z) = z(h_+ e^{-\lambda_+ z} - h_- e^{-\lambda_- z}). \tag{30}$$

with $h_+ > h_-$ and $\lambda_+ > \lambda_-$. This potential satisfies the requirement $h(z) \to 0$ for $z \to 0$ following from the location of the surface of the electrode at $z = 1/2$. For the above $h(z)$, the solution of (19) takes the form

$$\Delta c(z) = -h_+ e^{-\lambda_+ z}(b_0^+ + b_1^+ z) + h_- e^{-\lambda_- z}(b_0^- + b_1^- z), \tag{31}$$

where the coefficients depend on $\lambda_\pm$ as well as on the ion–ion interactions and ρ_R through the parameters A_0, A_2, and A_4 in the EL eqn (19), and are given in the Appendix. The charge density for $Q_e = 0$ is shown in Fig. 8 for $T^* = 1/l_B = 0.5$, $\rho = 0.8$, and $h_+ = 1$, $h_- = 0.7$, $\lambda_+ = 1.1$ and $\lambda_- = 0.8$ in (30).

For an anionophilic uncharged electrode, we obtain a layer of anions at the electrode's surface that in the case of a large density of ions is followed by a layer of cations because of the strong electrostatic attraction. The cation-rich layer attracts in turn anions, and alternating layers with decreasing charge are formed with increasing distance from the electrode. The layer of anions adsorbed due to the selectivity of the uncharged electrode leads to the same distribution of ions at large distances from the electrode as in the case of a charged nonselective electrode.

The charge distribution induced by the selectivity of the uncharged electrode leads to the PZC that is shown in Fig. 9 for the considered example of the electrode–ion interactions. We verified that for different forms of the interactions $h(z)$, the dependence of Ψ_{PZC} on the specific ion–ion interactions is nonmonotonic too, and the largest magnitude is taken for $\varepsilon^* \approx 0.7$. As shown in Fig. 6, the density of 'free' ions, ρ_R, takes a maximum for the same value of ε^*. From the mathematical point of view, Ψ_{PZC} depends on Δc, and Δc depends in particular on A_0 that is a function of ρ_R. In Section III A we

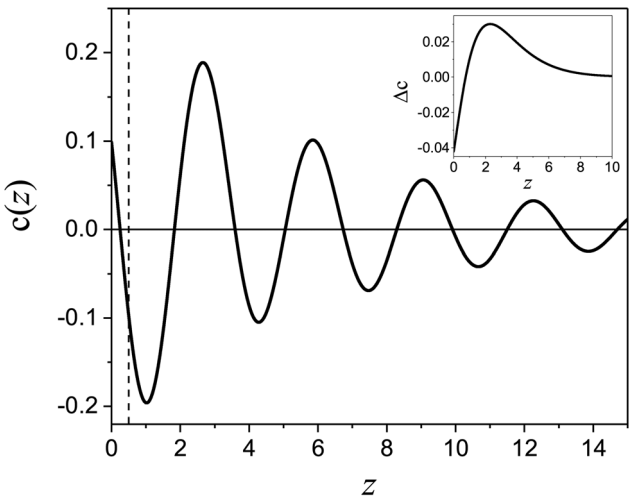

Fig. 8 The dimensionless charge density profile at the uncharged electrode (Q_e = 0) for T^* = 1/l_B = 0.5, ρ = 0.8, the strength of the specific ion–ion interactions ε^* = 1 and the potential $h(z)$ given in (30) with h_+ = 1, h_- = 0.7, λ_+ = 1.1 and λ_- = 0.8. z is in units of the ion diameter. The vertical dashed line at z = 1/2 indicates the position of the surface of the electrode. The behaviour of $\Delta c(z)$ is shown in the inset. For $0 < z < 1$, $c(z)$ contains contributions from the ions and the surface charge, because in our mesoscopic theory the charge is homogeneously distributed over the ionic core and $c(z)$ is proportional to the difference between the fraction of the layer with the thickness 1 and the mid-plane at z that is occupied by the cations and the anions (see Fig. 4).

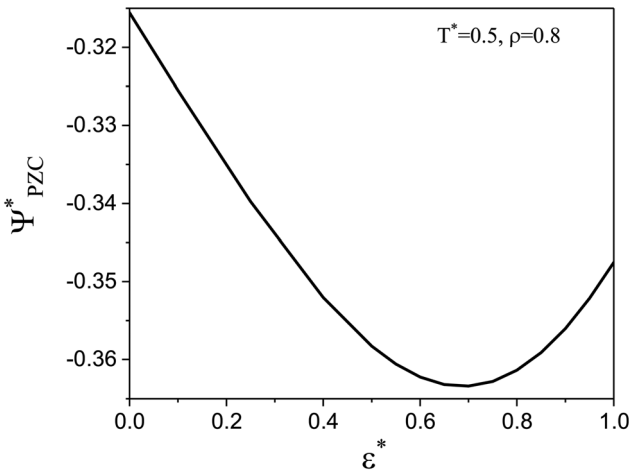

Fig. 9 The PZC in $4\pi e/a$ units for T^* = 1/l_B = 0.5, ρ = 0.8 and the potential $h(z)$ given in (30) with h_+ = 1, h_- = 0.7, λ_+ = 1.1 and λ_- = 0.8. The strength of the ion–ion interaction ε^* is in E_C units.

argued that the specific interactions counteract the charge-ordering induced by the Coulomb forces, and that for $\varepsilon^* \approx 0.7$ a crossover between alternating charged monolayers and bilayers occurs. Instantaneous distributions of ions differ strongly from the smooth average distribution in this case, and because of weaker ordering, more 'free' ions are present and contribute to the PZC.

D. Discussion

Predictions of our theory concern the ratio C/C_H between the double-layer capacitance of concentrated electrolytes, molten salts, IL and IL mixtures, and the Helmholtz capacitance $C_H = \epsilon_0 r/a$. The ratio C/C_H (see (26) and (27)) depends only on the decay length $1/\alpha_0$ and wavenumber α_1 of the exponentially damped charge oscillations (see (29)). α_0 and α_1 obtained in our theory in $1/a$ units can be compared with the corresponding parameters determined relatively easily in atomistic simulations and experiments. The Helmholtz capacitance, however, depends on the relative dielectric constant ϵ_r and the average diameter a of the ions that are input parameters in our theory. Unfortunately, determination of ϵ_r in the double-layer region is problematic, and it is difficult to find reliable data in the literature. In addition, in the case of the strongly asymmetric shape of ions that is typical for many IL, their different orientations in the layers parallel to the electrode lead to different thicknesses of these layers. Because the double-layer capacitance depends strongly on ϵ_r and a, we must compare our results with the existing data for the double-layer capacitance, ϵ_r and a that have limited accuracy and are often different in different sources.

Nevertheless, here we try to compare our predictions with experiment and atomistic simulations. We first note that swelling of alternating charged layers in the presence of strong SR interactions predicted by our theory was indeed observed experimentally in the case of the lithium bis(trifluoromethanesulfonyl)imide (LiTFSI) salt in water.[20,21] In this water-in-salt electrolyte, the SR interactions induce aggregation of the hydrophobic anions into bilayers separated by layers of hydrated Li^+ ions. In ref. 22 we obtained α_0 = 0.225 and α_1 = 1.613 in the same type of mesoscopic theory, but with the size-asymmetry of ions explicitly taken into account. These inverse lengths are in fair agreement with previous experiment,[21] and inserted into (26) give

$$C/C_H = 1.06. \quad (32)$$

Assuming $a \sim 1$ nm leading to $C_H \approx 0.9\epsilon_r$ μF cm^{-2} we obtain $C \approx 0.95\epsilon_r$ μF cm^{-2}. MD simulations give C = 5.6 μF cm^{-2} and C = 10 μF cm^{-2} for negative and positive charge electrodes because of different ionic sizes.[42] Typical values of ϵ_r in IL, $\epsilon_r \sim 10$ gives $C \approx 9.5$ μF cm^{-2}. In the present simplified theory the large size difference is not accounted for and quantitative agreement is not expected.

Another example of a common IL is 1-butyl-3-methylimidazolium tetrafluoroborate ([BMIM][BF4]), for which the results of atomistic simulations were fitted to (29) with α_0 = 1.2 nm^{-1} and α_1 = 10.3 nm^{-1}. The ions are elongated and the simulations indicate that the long axis is parallel to the electrode, therefore we assume a = 0.4 nm, and obtain

$$C/C_H = 2.887 \quad (33)$$

which with $C_H = 2.25\epsilon_r$ μF cm^{-2} gives $C = 6.5\epsilon_r$ μF cm^{-2}. In the simulations, $T \approx 298$ K, and $\epsilon_r = 1$ was assumed. Experimental result for the capacitance at room temperature of [BMIM][BF4] is $C \approx 6.5$ μF cm^{-2}.[43] In the bulk, $\epsilon_r \approx 10$ in this system, but the value of ϵ_r near an electrode can be significantly reduced.[10,44,45]

It should be noted that in the electrode–electrolyte systems, the total capacitance is given by $1/C = 1/C_{DL} + 1/C_{EL}$.[43,46,47] Our theory concerns only the double layer capacitance C_{DL}. The contribution $1/C_{EL}$ coming from the electrode is material dependent and requires separate consideration that is beyond the scope of this work.

To summarize, we obtain a semiquantitative agreement with atomistic simulations and experiment even in the very complex systems. However, the contribution to the capacitance associated with the distribution of ions near an electrode should be supplemented with predictions from a microscopic theory for the dielectric constant in the double layer to allow for a quantitative comparison with experimental results for C. Alternatively, precise experimental data for C, ϵ_r and a in the same system under the same conditions is necessary.

The PZC increases with increasing moments of $\Delta c(z)$ that in turn is an increasing function of the specific interactions between the ions and the electrode. This result is in agreement with experiments, where the selectivity of the electrode is identified with the selective adsorption at the uncharged electrode that in our theory is described by $\Delta c(z)$.[43] We observed also the dependence of the PZC on the SR interactions between the ions, and our conclusion that the PZC increases with increasing number of 'free' ions is also in line with experimental observations.[43]

IV. Concluding remarks

In the first part of the article, we improved the definition of the double-layer capacitance derived for concentrated ionic systems in ref. 11 within the mesoscopic theory. Here, we propose a definition of the charge of the electrode, eqn (25), consistent with the construction of the mesoscopic theory. We obtain perfect agreement with the Debye capacitance for dilute electrolytes, and for concentrated ones we obtain for C eqn (26) with (27) that is in fair quantitative agreement with simulations for the RPM.

In the second part we consider the RPM model with additional SR attractions between ions of the same charge and with specific ion–electrode interactions. We show that the double-layer capacitance at the PZC, C is given by the same simple formula as in the RPM (eqn (26)). This means that C/C_H at the PZC depends on the SR only through the inverse lengths α_0 and α_1 characterising the bulk structure, and is independent of the ion–electrode interactions. This result confirms that it is justified to compare theoretical results obtained with neglected ion–electrode interactions for the potential $\Psi(0)$ with the experimental results obtained for $\Psi(0) - \Psi_{PZC}$.

Because the same expression was obtained for the pure RPM and also for the RPM+SR systems, the formula (26) for the capacitance at the PZC is generally valid and can be applied to any ionic system with oscillatory decay of the charge–charge correlations. The ion–ion interactions, however, have a rather strong effect on the inverse lengths α_0 and α_1 (Fig. 6) and hence on C. When like ions attract one another with short-range forces, the capacitance at the PZC decreases, as shown in Fig. 7.

We obtained the PZC in terms of the charge profile for the ion–electrode interactions $h(z)$ of a general form, and illustrated our result on a particular example of anionophilic electrode. The absolute value of the Ψ_{PZC} takes a maximum for the strength of the specific ion–ion interactions that counteracts the charge ordering into neutral aggregates, thus leading to the largest density of 'free' ions.

Conflicts of interest

There are no conflicts of interest to declare.

Data availability

All formulas derived in this work are included in the article and the appendix. The figures were obtained from these formulas. No other data were used.

Appendices

Appendix

A Estimation of the strength of the SR interactions in imidazoilum based IL–water mixtures. From (23) we have the expression for the ratio of the strength of the SR interactions and the Coulomb potential between the ions at contact

$$\varepsilon^* \approx \frac{3.24\dfrac{\partial^2 \beta f_h}{\partial \rho_c^2} k_B T_c}{5.6\pi E_C} \tag{34}$$

where we used $\alpha = 1.8$, E_C is defined in (4) and T_c and ρ_c denote the critical temperature and density of ions. From ref. 25 we have $T_c \approx 420$ K for 1-alkyl-3-methylimidazolium bis{(trifluoromethyl)sulfonyl}imides. We use the Carnahan–Starling approximation for $\beta f_h(\rho)$ and the corresponding critical density $\rho_c \approx 0.25$. There is some ambiguity in defining $a = (a_+ + a_-)/2$, because the diameter of the cations depends strongly on conformation. We assume $a \approx 1$ nm and using $\epsilon = 4\pi\epsilon_0\epsilon_r$ obtain $\varepsilon^* \approx 0.05\epsilon_r$. We next assume that the static dielectric constant ϵ_r at the critical concentration is $\epsilon_r \approx 20$ and finally obtain $\varepsilon^* \approx 1$. The above estimations indicate that the ratio between the amplitude of the SR interactions in (5) and the Coulomb potential between monovalent bulky ions at contact is in the order of unity in physically relevant substances. In the case of simple salts like NaCl, we expect $\varepsilon^* < 1$.

B Parameters in the charge-profile near a selective electrode. The inverse decay length of the charge–charge correlations in the approximation (16) is given by

$$\alpha_0^{-2} = 2\frac{\beta v k_0^2 + \sqrt{(\beta v)^2 k_0^4 + \beta v \tilde{C}_a(k_0)}}{\tilde{C}_a(k_0)}$$

The phase θ and the amplitude A in $c_0(z)$ in the presence of the specific electrode–ion interactions satisfy the following

equations

$$\frac{A\alpha_1 \cot\theta}{\alpha_0^2+\alpha_1^2} = I_1(0) - \frac{A\alpha_0}{\alpha_0^2+\alpha_1^2}$$

and

$$Af = \mathrm{e}^{-\alpha_0/2}\left[\frac{\alpha_0}{\alpha_1}\sin(\alpha_1/2)+\cos(\alpha_1/2)\right]I_1(0) - I_1(1/2) + Q_\mathrm{e}$$

where f is given in (27), and we used (25).

The coefficients in (31) take the forms

$$b_0^{\pm} = 2\lambda_{\pm}(2A_4\lambda_{\pm}^2 + A_2)(b_1^{\pm})^2,$$

$$b_1^{\pm} = (A_4\lambda_{\pm}^4 + A_2\lambda_{\pm}^2 + A_0)^{-1},$$

and A_0, A_2, and A_4 are given by (20)–(22).

References

1 P. W. Debye and E. Hückel, Zur Theorie der Elektrolyte. I. Gefrierpunktserniedrigung und verwandte Erscheinungen, *Phys. Z.*, 1923, **24**, 185–206.
2 J. L. Barrat and J. P. Hansen, *Basic Concepts for Simple and Complex Liquids*, Cambridge University Press, 2003.
3 R. J. F. L. de Carvalho and R. Evans, The decay of correlations in ionic fluids, *Mol. Phys.*, 1994, **83**, 619–654.
4 M. V. Fedorov and A. A. Kornyshev, Ionic liquid near a charged wall: structure and capacitance of electrical double layer, *J. Phys. Chem. B*, 2008, **112**, 11868–11872.
5 M. V. Fedorov and A. A. Kornyshev, Ionic liquids at electrified interfaces, *Chem. Rev.*, 2014, **114**, 2978.
6 J. M. Otero-Mato, H. Montes-Campos, O. Cabeza, D. Diddens, A. Ciach and L. J. Gallego, *et al.*, 3D Structure of the Electric Double Layer of Ionic Liquid-Alcohol Mixtures at the Electrochemical Interface, *Phys. Chem. Chem. Phys.*, 2018, **20**, 30412.
7 A. Ciach and O. Patsahan, Structure of ionic liquids and concentrated electrolytes from a mesoscopic theory, *J. Mol. Liq.*, 2023, **377**, 121453.
8 R. M. Adar, S. A. Safran, H. Diamant and D. Andelman, Screening length for finite-size ions in concentrated electrolytes, *Phys. Rev. E*, 2019, **100**(4), 042615.
9 A. Ciach and O. Patsahan, Correct scaling of the correlation length from a theory for concentrated electrolytes, *J. Phys.: Condens. Matter*, 2021, **33**, 37LT01.
10 S. Park and J. G. McDaniel, Generalized Helmholtz model describes capacitance profiles of ionic liquids and concentrated aqueous electrolytes, *J. Chem. Phys.*, 2024, **160**(16), 164709.
11 A. Ciach and O. Patsahan, Mesoscopic theory for a double layer capacitance in concentrated ionic systems, *Phys. Chem. Chem. Phys.*, 2025, **27**, 9143–9151.
12 M. V. Fedorov and A. A. Kornyshev, Towards understanding the structure and capacitance of electrical double layer in ionic liquids, *Electrochim. Acta*, 2008, **53**, 6835–6840.
13 C. Cruz, A. Ciach, E. Lomba and S. Kondrat, Electrical double layers close to ionic liquid-solvent demixing, *J. Phys. Chem. C*, 2019, **123**, 1596–1601.
14 A. Iglič, E. Gongadze and V. Kralj-Iglič, Differential capacitance of electric double layer – influence of asymmetric size of ions, thickness of stern layer and orientational ordering of water dipoles, *Acta Chim. Slov.*, 2019, **66**(3), 534–541.
15 J. Yang, S. Kondrat, C. Lian, H. Liu, A. Schlaich and C. Holm, Solvent Effects on Structure and Screening in Confined Electrolytes, *Phys. Rev. Lett.*, 2023, **131**(11), 118201.
16 M. Dinpajooh, E. Biasin, E. T. Nienhuis, S. T. Mergelsberg, C. J. Benmore and G. K. Schenter, *et al.*, Detecting underscreening and generalized Kirkwood transitions in aqueous electrolytes, *J. Chem. Phys.*, 2024, **161**, 151102.
17 K. Sadakane, A. Onuki, K. Nishida, S. Koizumi and H. Seto, Multilamellar structures induced by hydrophilic and hydrophobic ions added to a binary mixture of D_20 and 3-methylpyridine, *Phys. Rev. Lett.*, 2009, **103**, 167803.
18 J. Leys, D. Subramanian, E. Rodezno, B. Hammouda and M. A. Anisimov, Mesoscale phenomena in solutions of 3-methylpyridine, heavy water, and an antagonistic salt, *Soft Matter*, 2013, **9**, 9326.
19 F. Pousaneh, A. Ciach and A. Maciołek, How ions in solution can change the sign of the critical Casimir potential, *Soft Matter*, 2014, **10**, 470–483.
20 O. Borodin, L. Suo, M. Gobet, X. Ren, F. Wang and A. Faraone, *et al.*, Liquid Structure with Nano-Heterogeneity Promotes Cationic Transport in Concentrated Electrolytes, *ACS Nano*, 2017, **11**, 10462.
21 T. Groves, C. S. Perez-Martinez, R. Lhermerout and S. Perkin, Surface forces and structure in a water-in-salt electrolyte, *J. Phys. Chem. Lett.*, 2021, **12**, 1702–1707.
22 O. Patsahan and A. Ciach, Mesoscopic inhomogeneities in concentrated electrolytes, *ACS Omega*, 2022, **7**, 6655.
23 S. Wang, H. Tao, J. Yang, J. Cheng, H. Liu and C. Lian, Structure and Screening in Confined Electrolytes: The Role of Ion Association, *J. Phys. Chem. Lett.*, 2024, **33**, 7147.
24 W. Schröer and V. R. Vale, Liquid–liquid phase separation in solutions of ionic liquids: phase diagrams, corresponding state analysis and comparison with simulations of the primitive model, *J. Phys.: Condens. Matter*, 2009, **21**, 424119.
25 J. Rotrekl, J. Storch, P. Velíšek, W. Schröer, J. Jacquemin and Z. Wagner, *et al.*, Liquid Phase Behavior in Systems of 1-Butyl-3-alkylimidazolium bis(trifluoromethyl)sulfonyl imide Ionic Liquids with Water: Influence of the Structure of the C5 Alkyl Substituent, *J. Solution Chem.*, 2017, **46**, 1456–1474.
26 D. Chandler, Interfaces and the driving force of hydrophobic assembly, *Nature*, 2005, **437**, 7059.
27 C. Merlet, M. Salanne, B. Rotenberg and P. A. Madden, Imidazolium Ionic Liquid Interfaces with Vapor and Graphite: Interfacial Tension and Capacitance from Coarse-Grained Molecular Simulations, *J. Phys. Chem. C*, 2011, **115**, 16613.
28 J. Yang, Y. Ding, C. Lian, S. Ying and H. Liu, Theoretical Insights into the Structures and Capacitive Performances of Confined Ionic Liquids, *Polymers*, 2020, **12**, 722.
29 J. N. Itliong, A. L. Frischknecht, M. J. Stevens and I. Nakamura, Stockmayer fluid simulations for viscosity and glass transition temperature of ionic liquids, *J. Chem. Phys.*, 2025, **163**, 044503.

30 N. F. Carnahan and K. E. Starling, Equation of state for nonattracting rigid spheres, *J. Chem. Phys.*, 1969, **51**, 635.
31 R. Kjellander, Focus Article: Oscillatory and long-range monotonic exponential decays of electrostatic interactions in ionic liquids and other electrolytes: The significance of dielectric permittivity and renormalized charges, *J. Chem. Phys.*, 2018, **148**(19), 193701.
32 R. Kjellander, The intimate relationship between the dielectric response and the decay of intermolecular correlations and surface forces in electrolytes, *Soft Matter*, 2019, **15**, 5866.
33 N. Bjerrum, Ionic association. I. Influence of ionic association on the activity of ions, *Kgl. Dan. Vidensk. Selsk. Math. Fys. Medd.*, 1926, **7**, 1–48.
34 M. E. Fisher and Y. Levin, Criticality in ionic fluids: Debye-Hückel theory, Bjerrum, and beyond, *Phys. Rev. Lett.*, 1993, **71**, 3826–3829.
35 G. Stell and Y. Zhou, Chemical association in simple models of molecular and ionic fluids, *J. Chem. Phys.*, 1989, **91**(6), 3618–3623.
36 M. F. Holovko and Y. V. Kalyuzhnyi, On the effects of association in the statistical theory of ionic systems. Analytic solution of the PY-MSA version of the Wertheim theory, *Mol. Phys.*, 1991, **73**(5), 1145–1157.
37 L. Blum and O. Bernard, The general solution of the binding mean spherical approximation for pairing ions, *J. Stat. Phys.*, 1995, **79**(3–4), 569–583.
38 A. Ciach, Simple theory for oscillatory charge profile in ionic liquids near a charged wall, *J. Mol. Liq.*, 2018, **270**, 138.
39 C. Bacon, A. Serva, C. Merlet, P. Simon and M. Salanne, On the key role of electrolyte–electrode van der Waals interactions in thesimulation of ionic liquids-based supercapacitors, *Electrochim. Acta*, 2023, **455**, 142380.
40 J. G. Kirkwood, Statistical mechanics of liquid solutions, *Chem. Rev.*, 1936, **19**, 275–307.
41 A. Ciach, W. T. Góźdź and R. Evans, Effect of a nearby charge-ordered phase on correlation functions in ionic systems, *J. Chem. Phys.*, 2003, **118**, 3702.
42 Z. Li, G. Jeanmairet, T. Méndez-Morales, B. Rotenberg and M. Salanne, Capacitive Performance of Water-in-Salt Electrolytes in Supercapacitors: A Simulation Study, *J. Phys. Chem. C*, 2018, **122**, 23917.
43 V. Lockett, M. Horne, R. Sedev, T. Rodopoulos and J. Ralston, Differential capacitance of the double layer at the electrode/ionic liquids interface, *Phys. Chem. Chem. Phys.*, 2010, **12**, 12499.
44 L. Fumagalli, A. Esfandiar, R. Fabregas, S. Hu, P. Ares and A. Janardanan, *et al.*, Anomalously low dielectric constant of confined water, *Science*, 2018, **360**(6395), 1339–1342.
45 A. V. Dubtsov, S. V. Pasechnik, D. V. Shmeliova, A. S. Saidgaziev, E. Gongadze and A. Iglič, *et al.*, Liquid crystalline droplets in aqueous environments: electrostatic effects, *Soft Matter*, 2018, **14**(47), 9619–9630.
46 W. Schmickler, Electronic Effects in the Electric Double Layer, *Chem. Rev.*, 1996, **96**(8), 3177–3200.
47 G. Jeanmairet, B. Rotenberg and M. Salanne, Microscopic Simulations of Electrochemical Double-Layer Capacitors, *Chem. Rev.*, 2022, **122**(12), 10860–10898.

